Superior Microstructure of High-Performance Concrete for Long-Term Durability

DELLA M. ROY, MICHAEL R. SILSBEE, SCOTT SABOL, AND BARRY E. SCHEETZ

Recent advances in using calculated packing diagrams to optimize cement and concrete materials offer the promise of superior product characteristics achieved by increased packing efficiency. A high packing efficiency with adequate mixing and placing techniques results in the formation of a fine microstructure that results in low permeability. The low permeability causes increased resistance to aggressive forces from the environment, which together enhance its long-term durability. The favorable interaction among physical and chemical phenomena gives rise to better long-term performance, whether the application is structural, chemical (such as in waste management), or a combination (as in highway concrete).

High-performance concrete has been defined (*1*) as concrete in which some or all of the following properties have been enhanced:

- Ease of placement and compaction,
- Long-term mechanical properties,
- Early-age strength,
- Toughness,
- Volume stability, and
- Extended life in severe environments.

High strength is not necessarily a criterion for high-performance concrete, although many high-performance concretes exhibit superior mechanical properties. Three of the six criteria are concerned with the long-term behavior or durability of the concrete. Transport of fluids into or out of the pore structure of hardened concrete is the principal mechanism responsible for the deterioration of concrete (*2*). The transport of fluids and accompanying dissolved ionic species in hardened concrete may be considered in terms of permeability.

This paper focuses on high-performance cementitious materials designed for durability. First, some of the fundamentals of porosity and permeability of cementitious systems and their relation to durability are examined. Then, factors that control the porosity and permeability in concretes are discussed. Finally, the effect of packing on properties, such as chloride permeability, is treated.

POROSITY AND PERMEABILITY IN HARDENED CEMENTITIOUS SYSTEMS

Assuming negligible volume change on curing, the total volume of a hardened portland cement paste will be the sum of the volumes of the anhydrous cement, water, and any entrapped air, or

$$V_t = V_s + V_l + V_a$$

where

V_t = total volume,
V_s = volume of anhydrous portland cement,
V_l = volume of liquid (water), and
V_a = volume of any entrapped air.

Another way of expressing V_t is

$$V_t = (W_s/\rho_s + W_l/\rho_l) + V_a$$

where

W_s = mass of anhydrous cement,
ρ_s = density of anhydrous cement,
W_l = mass of water, and
ρ_l = density of water.

Assuming $\rho_l = 1$, then

$$V_t = (W_s/\rho_s + W_l) + V_a$$

Each gram of anhydrous portland cement will combine chemically with approximately 0.25 g of water during hydration. Therefore, V_t becomes

$$V_t = [1.25W_s/\rho_h + (W_l - 0.25W_s)] + V_a$$

Where ρ_h = density of the hydrated solid.

The total volume of the pores in the hydrated cement pastes is then

$$V_p = (W_l - 0.25W_s) + V_a$$

As early as 1886 (*3*) the effect of water content on the strength of hardened concrete was recognized. The volume of pores thus calculated represents the capillary porosity, gel porosity, and entrapped air. From these three sources of porosity, only the capillary porosity will contribute to the fluid permeability of the hardened cement paste.

Ideally, the flow through a hardened portland cement paste may be expressed as

$$F/A = K\mu/(L \cdot \Delta P)$$

Pennsylvania State University, Materials Research Laboratory, University Park, Pa. 16802. Current affiliation of S. Sabol: Transportation Research Board, National Research Council, 2101 Constitution Avenue, N.W., Washington, D.C. 20418.

where

F = flow (L/sec),
A = cross-sectional area (m^2),
L = thickness of specimen (m),
K = permeability coefficient (m^2),
μ = viscosity of permeating fluid ($N \cdot sec/m^2$), and
ΔP = mean pressure (N/m^2).

For a cement paste it was concluded (*4,5*) that it was possible to block the capillary porosity with cement gel if the water-to-cement ratio in the paste is low. The limiting water-to-cement ratio required to block fluid flow is a function of curing time. At a ratio of 0.7, times of approximately 1 year are required; at a ratio of 0.4, the time required for the cement gel to block the capillary pores may be only 3 days.

A characteristic pore size is determined by mercury intrusion porosimetry was defined (*6*). The characteristic pore size was defined as the maximum on the derivative of the volume intruded versus pressure curve (dV/dP). A linear relationship between the log of the characteristic pore size and permeability was found. However, the coefficient of variation for the relationship was large (approximately 50 percent). More recent studies (7–9) have shown that a log-normal distribution or mixtures of log-normal distributions may be used to describe the pore structure of hardened cementitious materials. These studies defined a characteristic diameter based on the moment, $<D^2>$, of the log-normal distribution. The relationship between the characteristic diameter and permeability was found to be (*10*):

$$k = (f/32)p<D^2>$$

where

k = permeability,
f = fraction of connected porosity, and
p = porosity.

When the total porosity decreases and commonly the median pore size decreases, the rate-controlling mechanism for movement of ions through hardened cement pastes transforms from fluid flow to diffusion. The controlling relationship then obeys Fick's law:

$$\text{rate of diffusion} = -D\frac{dc}{dx}$$

where D is the diffusion coefficient, and dc represents a concentration gradient over distance dx.

DURABILITY

Table 1 lists the principal mechanisms that contribute to the shortening of the service life of hardened concretes. These degradation mechanisms can be classified into two categories—thermo-mechanical and chemical—although there is some interaction and overlapping of the two. The mechanisms highlighted in boldface type require a mass transport of ionic or molecular species into or out of the cementitious matrix. This transport occurs via movement through the conduits that connect the exterior of the concrete to the interior (that is, the system of pores). Therefore, both the total number of pores and the pore size distribution are important in controlling the performance of the concrete and hence its durability.

The preceding section discussed the formation of porosity. To develop durable concrete formulations, one must address the methods of modifying the total porosity and the pore size distribution by advanced placement procedures and proper selection of the constituents of the formulations based on particle size distributions and chemistry.

CONTROL OF POROSITY AND PERMEABILITY IN CONCRETES

Chemical Effects on Porosity and Permeability

The use of low water-to-solids (w-s) ratio formulations and mineral admixtures to increase the durability of hardened cementitious systems is well documented (*2,11–13*). With the proper selection of

TABLE 1 Degradation Processes

Thermo-mechanical	*Chemical*
	sulfate
pressure/temperature alteration of phase stability	**-- calcium**
freezing and thawing cycling	**-- magnesium**
wet and dry cycling	**-- sodium**
cracking	**chloride**
-- drying shrinkage	**carbonation**
-- metal corrosion	**alkali aggregate reaction**
-- stresses due to temperature changes	**leaching**
-- carbonation	
-- physical loading	

reactive mineral admixtures, a fair degree of control can be exercised over the performance of the concrete. Figure 1 demonstrates the effect of w-s, high-range water-reducing admixture (HRWRA), and mineral admixtures on porosity development in cementitious pastes.

Ground granulated (glassy) blast-furnace slag as an ingredient of the cement paste that can replace significant amounts of the portland cement has been developed and is currently a commercial product. The commonly accepted mechanism for hydrating slag is by activating the very finely ground glassy slag by portland cement hydration products, which results in a slow initial hydration reaction. Figure 2 contrasts mercury-intrusion porosimetry results obtained on freeze-dried specimens of an ordinary portland cement (OPC) paste and a 60:40 slag: OPC-blended cement paste both cured under identical conditions at 45°C for 14 days with a w-s of 0.4. The data, presented as the differential *dV/dP*, show that the OPC possesses a pore distribution that centers at about 12.5 nm, the so-called critical pore radius. In contrast, the blended slag cement reveals a pore-size distribution with a very broad maximum weakly centered at about 3.5 nm and extending from 12.5 to 2.0 nm. Figure 3 is a replot of these data in a cumulative pore volume form showing that both specimens had approximately the same total porosity (within about 5 to 6 percent) but distinctly different pore size distributions. In this example, the reactive additional ingredient (slag) has the characteristic of hydrating at a much slower rate, resulting in a significantly reduced pore size distribution, and at the same time not adversely affecting the 28-day mechanical properties of the concrete. Any number of other materials have the potential of performing similarly.

Degradation due to steel corrosion induced by chloride penetration is a common cause of concrete structure failures. Many

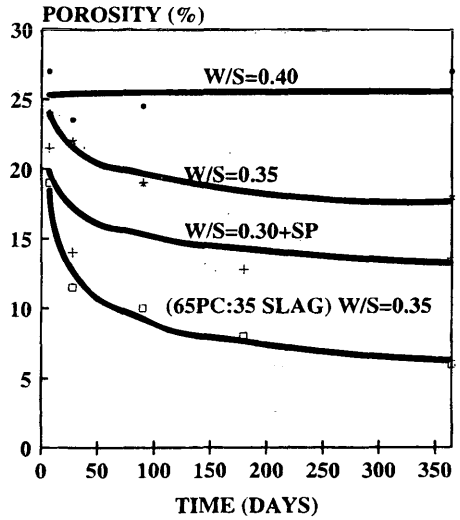

FIGURE 1 Effect of W/S (HRWRA) and mineral admixtures on porosity development in cementitious pastes (*13*).

investigations have been performed on the movement of chlorides through hardened cement pastes (*2,6,14–19*). In view of applications to radioactive waste management, the movement of Cs+ and Cl− ions through hardened cement pastes prepared using a variety of w-s and various slags and mineral admixtures was studied (*13*). Typical results for the diffusion of Cl ions are summarized in Table 2. Decreasing the w-s from 0.40 to 0.35 resulted in a decrease in the effective diffusion coefficient from 110 to 75.1 [($\times 10^{13}$) (m^2/sec)].

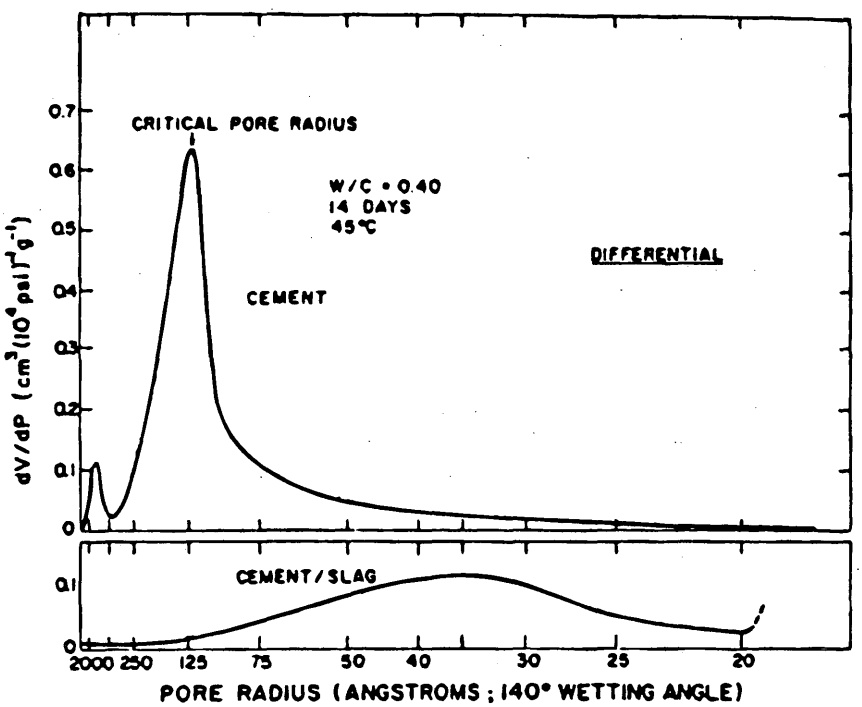

FIGURE 2 Comparison of mercury intrusion porosimetry results obtained on freeze-dried specimens of OPC and 60:40 slag (OPC blended cement both cured under identical conditions at 45°C for 14 days with w-s ratio of 0.4).

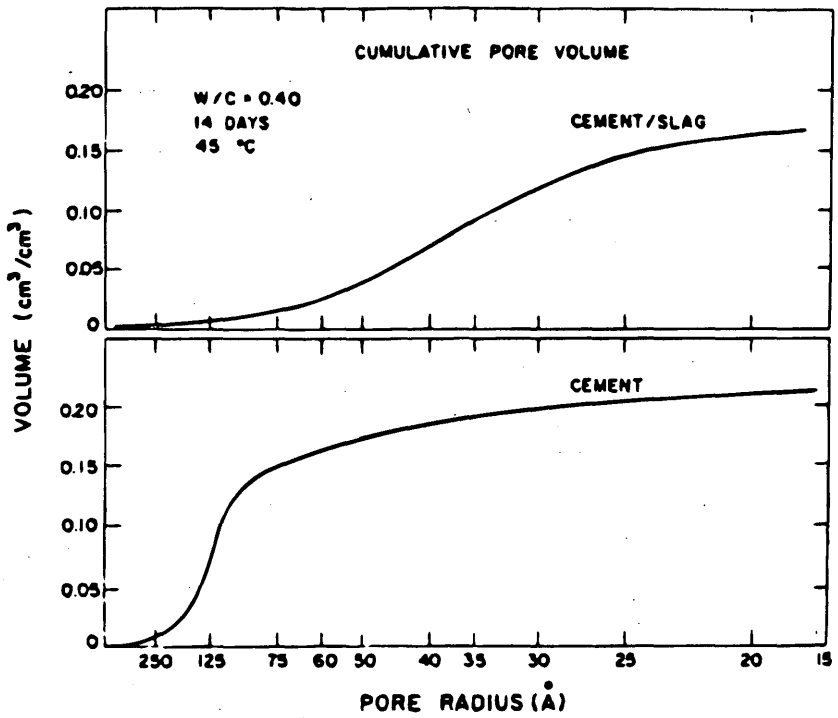

FIGURE 3 Replot of data in Figure 2 in cumulative pore volume form showing that both specimens had approximately same total porosity (within about 5 to 6 percent) but distinctly different pore size distributions.

Lower water contents result in lower total porosity and a more tortuous pore system. The addition of a small amount of a HRWRA further decreased the diffusion coefficient at the same w-s. Blast-furnace slag and silica fume proved the most effective in reducing the diffusion coefficient as compared with an OPC paste from 75.1 to 9.62 to 4.35, respectively. The effectiveness of blast-furnace slag and silica fume was attributed to increased calcium-silica-hydrate (C-S-H) production resulting in a filling of the pores. In both cases, using an HRWRA resulted in still a further decrease in the diffusion coefficient. The use of a low calcium fly ash as a mineral admixture proved much less effective in reducing chloride diffusion. The lower effectiveness of the fly ash as compared with slag and silica fume was attributed to the lesser reactivity of the lower calcium ash. Other studies (*14,17–19*) have shown similar results. Although the total porosity and median pore size remain the same as compared to OPC at normal curing temperatures, the reduction in the diffusion coefficient has been attributed to an increased number of finer pores. High-calcium content fly ashes have generally been found to be more effective at reducing chloride diffusion at early ages. Fly ashes have been shown to be more effective at elevated temperatures presumably as a result of higher reaction rates leading to increased C-S-H production. The results suggest that with elevated temperature curing or after a long curing time fly ash may still be an effective tool for reducing chloride diffusion (*16*).

Physical Effects on Porosity and Permeability

An integral part of the porosity that occurs in cementitious systems is attributable to the voids created among the dry components of the

TABLE 2 Effective Diffusion Coefficients for Cl^- in Water-Saturated Pastes at 25°C on Samples Cured for 28 Days at 25°C before Testing (*13*)

PASTE	W/S	D_{Cl^-}(X10^{13}) (m^2/sec)
OPC	0.40	110
OPC	0.35	75.1
OPC	0.35+SP*	60
OPC	0.30+SP	56.9
35% OPC + 65% SLAG	0.35	9.62
35% OPC + 65% SLAG	0.30+SP	8.61
90% OPC + 10% SILICA FUME	0.40	4.35
90% OPC + 10% SILICA FUME	0.35+SP	2.9
70% OPC + 30% FLY ASH	0.35	55.8
70% OPC + 30% FLY ASH	0.30+SP	43.8

* *with HRWRA addition*

formulation as well as the morphology of the individual components. Studies performed in Denmark (*11*) and the United States (*12*) demonstrated that significant improvement in mechanical properties of portland cement systems could be achieved using an approach based on the proper selection of concrete components to maximize space filling. The development of densified small particle (DSP) cements resulted in low interconnected porosity, very high compressive strengths, and a variety of additional outstanding properties, least of which is the retention of compressive strengths in thermal application in excess of 600°C that is about 65 percent of room temperature values (*20*).

A computer algorithm that has been used to help calculate concrete formulations with maximal density has been described (*9,21,22*). The algorithm requires as input size distributions and tap densities of the individual components. The size distributions for the fine components, such as cement, are determined using x-ray sedimentation techniques and for the coarse components by dry sieving. The tap density is determined by packing the dry component in a column with vibration. The bulk or tap density is then calculated based on the weight of the sample and the volume occupied in the column. The code is the implementation of two models reported in the open literature; one for large particles [Toufar model (*23*)] and one for small particles [(Aim model (*24*)].

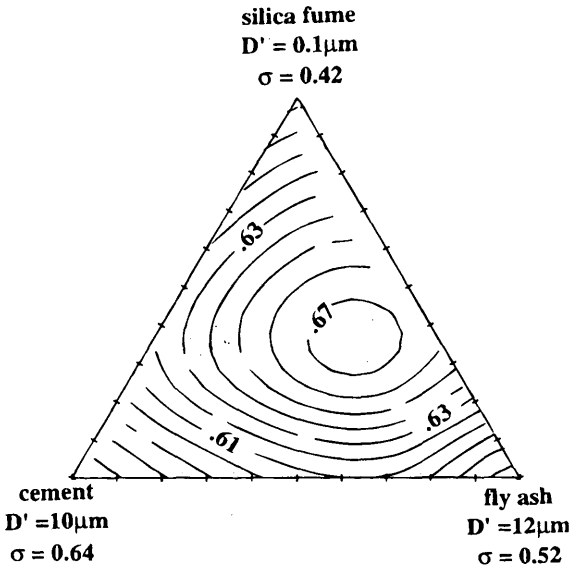

FIGURE 4 Packing diagram blend of 37.5, 19.0, and 9.5mm size-numbered coarse aggregate with input from Table 5.

Use of Reactive Mineral Admixtures and Tailored Aggregate Mixtures.

Increasingly large numbers of concrete formulations are being proportioned with some form of reactive mineral admixture. Each component of the concrete formulation—cement, fine, and coarse aggregate—can in turn be optimized to ensure the densest possible formulation. Caution must be exercised when using this approach. The densest formulation may not be desirable, and its use must be tempered by practical knowledge of reactivity and desired physical properties. Figure 4 represents the use of one such packing diagram for blending cementitious constituents in a concrete. Table 3 summarizes the input data used to generate Figure 4.

Maximum packing for this example suggests an optimal blending, which is summarized in Table 4. As can be seen, the maximum packing density does not necessarily correspond to where one would normally select a cementitious blend; it contains slightly more silica fume and less fly ash than desirable from the standpoint of chemistry and rheology. Figure 5 is a comparable packing diagram blend of 37.5 mm, 19.0 mm, and 9.5 mm size-numbered coarse aggregate with input from Table 5.

ASTM C 33—Standard Specification for Concrete Aggregates

Using the dry packing model allows for a critical evaluation of the existing size-number designation grading requirements. It also facilitates analysis of the effects of those gradings on subsequent dependent specifications, such as ACI 211.11. This analysis should enhance the quality control in the production of high-performance concrete.

Analysis of the grading requirements for coarse aggregates contained in Table 2 of ASTM C 33 (Figure 6) was carried out in the

TABLE 3 Input Data for Packing Calculation of Cementitious Components

	*characteristic size** (μm)	*tap density*
silica fume	**0.1**	**0.42**
cement	**10**	**0.64**
fly ash	**12**	**0.52**

* *determined from the D50 value.*

TABLE 4 Optimal Packing for Cementitious Components

	density (Mg/m^3)	*volume percent*	*mass percent*
silica fume	**2.1**	**22**	**16**
cement	**3.1**	**72**	**79**
fly ash	**2.35**	**6**	**5**

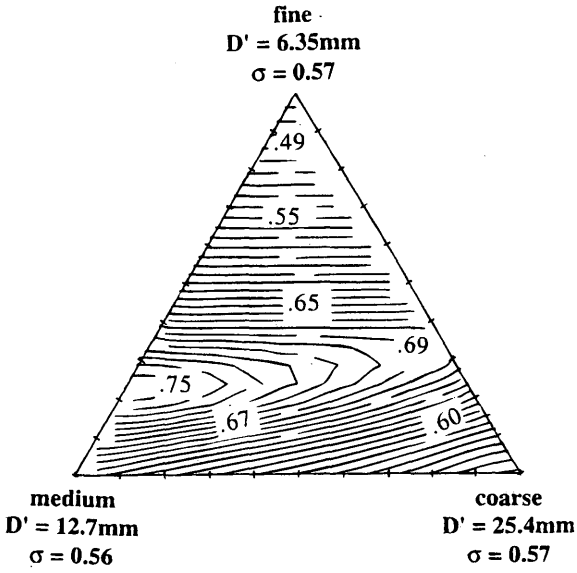

FIGURE 5 Use of packing diagram for blending of cementitious constituents in concrete. Table 3 summarizes input data used to generate this figure.

following manner. For each size-number designation, five different combinations of the size fractions were developed. One combination emphasized the largest allowable aggregate sizes for a size-number. The second combination emphasized the aggregate size in the middle-size ranges for the same specified size-number. A third combination consisted of the highest percentage allowable for the smallest aggregate in the size-number designation, with minimum of medium- or large-sized aggregate. The fourth combination resulted from combining of the largest and the smallest size-number fractions, but minimizing the percentage from the medium sizes. The final combination was developed using the mean value of the existing allowable percentages in each of the size-fraction designations.

These five combinations were input into the packing algorithm, and plots of iso-densities were determined for a concrete formulation consisting of cement and fine and coarse aggregate. Coarse aggregate was chosen as the variable for this study because of its greater influence on the binary packing of the fine and coarse aggregate (*25*).

It was observed that some of the combinations described for each size-number designation resulted in poor packing density characteristics and therefore in poorer concretes. These poor packing characteristics within a size-number designation include combinations that (a) result in a noticeably lower maximum packing density than other combinations, (b) result in very small regions of comparable packing density, or (c) have gradients in packing density in the directions of increasing or decreasing volume percentages of fine or coarse aggregate, or all. This final characteristic would result in little tolerance for error in aggregate proportioning during the batching process that could lead to large changes in the concrete and therefore affect the initial and final concrete properties.

An encouraging outcome of the study is noted in all of the combinations within a size-numbered designation. There is a certain arbitrary level of packing that is the same in value and roughly in the same area and location for all of the combinations evaluated. An example of this phenomenon is demonstrated by comparing the shaded regions of panels (a), (b), and (c) of Figure 7. Note that although the maximum packing density value and position are different for all three combinations, the density plateau labeled 0.87 is generally the same in area, shape, and position for all three. This similarity suggests that, in practice, this iso-density limit would be the lowest level of packing expected regardless of the proportioning of size fractions in the coarse aggregate size-number (based on these combinations of concrete components). It is only the characteristics of the packing densities above this "base level" that are affected by the various combinations analyzed here. Although these observations could result in improvements to the use of coarse aggregates in concrete, it is reassuring that the packing model helps to explain the generally acceptable results obtained using the current ASTM C 33 gradings.

Effects of Natural Versus Manufactured Aggregates on Packing Density

The efficiency with which the dry constituents of a concrete formulation can be assembled depends on the morphology of the particles. Angularity and aspect ratio are not specifically measured for input into the packing model described elsewhere (*9,22*) but are indirectly included in the tap density. An aggregate that meets the C 33 grading guidelines and has been prepared by crushing, when contrasted with a similar aggregate that occurs naturally and does not require crushing, will exhibit different packing behavior. An angular to subangular aggregate will not pack as densely as its rounded to subrounded counterpart. Figure 8 contrasts the differences in packing that are calculated for a no. 8 manufactured limestone aggregate with the same cement and fine aggregate prepared from a rounded natural quartz aggregate. The differences in dry packing for these two systems can be as much as 8 to 10 volume percent.

Effect of Packing on Chloride Permeability

The effect of packing density on durability and, in particular, transport properties of species into or out of the concrete is reflected in measurements such as that of chloride permeability. Some experimental studies were undertaken to evaluate this effect. The chloride permeability of concrete specimens was measured by monitoring the net charge (coulombs) passing in 6 hr through a cylinder

TABLE 5 Input Data for Packing Calculation of Coarse Aggregate

	characteristic size (mm)	*tap density*
fine	6.35	0.57
medium	12.7	0.56
coarse	25.4	0.57

Size Number	Nominal Size (Sieves with Square Openings)	Amounts Finer than Each Laboratory Sieve (Square-Openings), Weight Percent												
		4 in. (100 mm)	3½ in. (90 mm)	3 in. (75 mm)	2½ in. (63 mm)	2 in. (50 mm)	1½ in. (37.5 mm)	1 in. (25.0 mm)	¾ in. (19.0 mm)	½ in. (12.5 mm)	⅜ in. (9.5 mm)	No. 4 (4.75 mm)	No. 8 (2.36 mm)	No. 16 (1.18 mm)
1	3½ to 1½ in. (90 to 37.5 mm)	100	90 to 100	...	25 to 60	...	0 to 15	...	0 to 5	...	...	...	...	...
2	2½ to 1½ in. (63 to 37.5 mm)	...	...	100	90 to 100	35 to 70	0 to 15	...	0 to 5	...	...	...	...	...
3	2 to 1 in. (50 to 25.0 mm)	...	...	...	100	90 to 100	35 to 70	0 to 15	...	0 to 5	...	...	...	...
357	2 in. to No. 4 (50 to 4.75 mm)	...	...	...	100	95 to 100	...	35 to 70	...	10 to 30	...	0 to 5	...	...
4	1½ to ¾ in. (37.5 to 19.0 mm)	...	...	...	...	100	90 to 100	20 to 55	0 to 15	...	0 to 5	...	...	...
467	1½ in. to No. 4 (37.5 to 4.75 mm)	...	...	...	...	100	95 to 100	...	35 to 70	...	10 to 30	0 to 5	...	...
5	1 to ½ in. (25.0 to 12.5 mm)	...	...	...	...	...	100	90 to 100	20 to 55	0 to 10	0 to 5	...	...	...
56	1 to ⅜ in. (25.0 to 9.5 mm)	...	...	...	...	...	100	90 to 100	40 to 85	10 to 40	0 to 15	0 to 5	...	...
57	1 in. to No. 4 (25.0 to 4.75 mm)	...	...	...	...	...	100	95 to 100	...	25 to 60	...	0 to 10	0 to 5	...
6	¾ to ⅜ in. (19.0 to 9.5 mm)	...	...	...	...	...	...	100	90 to 100	20 to 55	0 to 15	0 to 5	...	...
67	¾ in. to No. 4 (19.0 to 4.75 mm)	...	...	...	...	...	...	100	90 to 100	...	20 to 55	0 to 10	0 to 5	...
7	½ in. to No. 4 (12.5 to 4.75 mm)	...	...	...	...	...	...	...	100	90 to 100	40 to 70	0 to 15	0 to 5	...
8	⅜ in. to No. 8 (9.5 to 2.36 mm)	...	...	...	...	...	...	...	...	100	85 to 100	10 to 30	0 to 10	0 to 5

FIGURE 6 Table 2 of ASTM C 33.

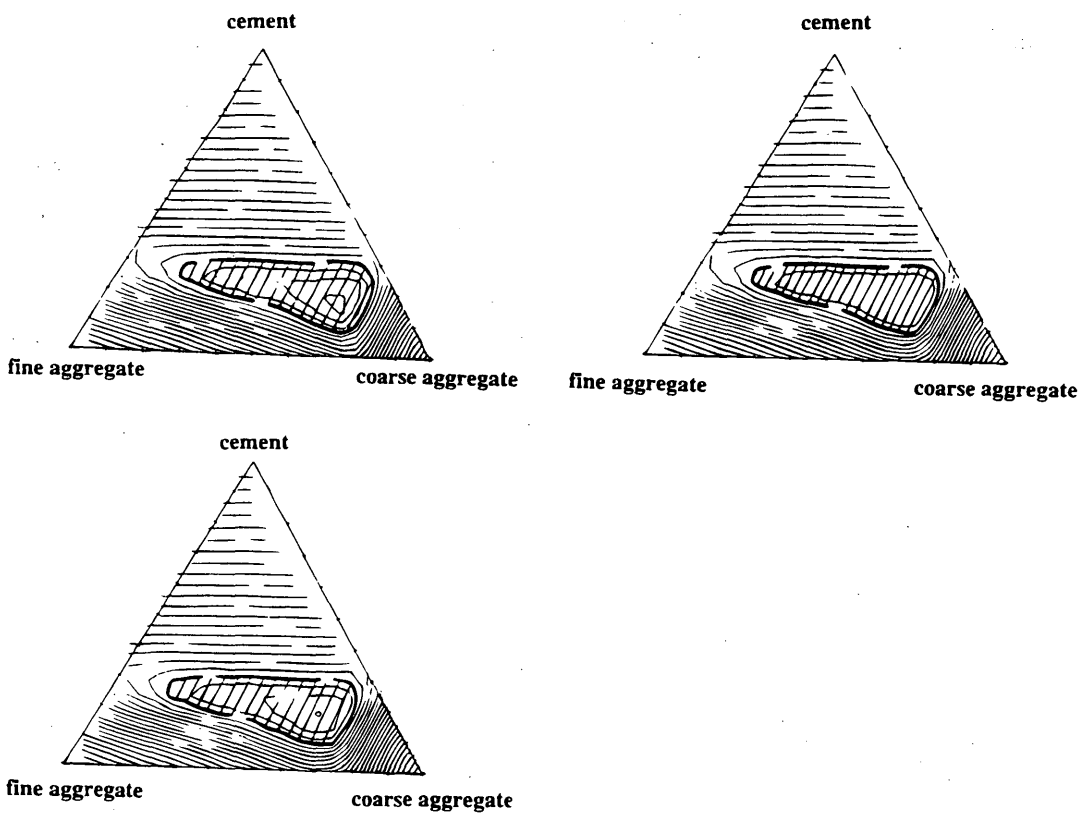

FIGURE 7 Dry packing calculation of cement, fine aggregate, and coarse aggregate with varying proportions of sizes within coarse aggregate.

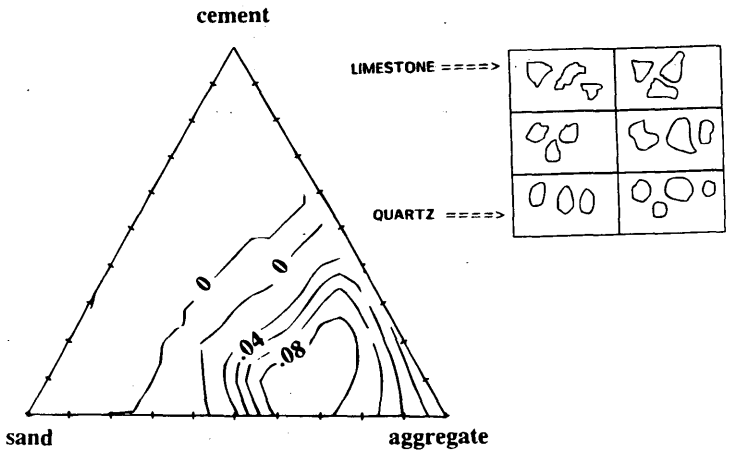

FIGURE 8 Difference between iso-density lines for two concretes composed of cement, sand, and no. 8 coarse aggregate. Differences expressed present effects on packing density between angular, manufactured limestone and natural, subround morphology of quartz aggregate.

(95.25ϕ× 51 mm) mounted in a cell with two compartments, filled with NaCl and NaOH solutions, under the influence of 60 V dc electrical potential (AASHTO T–277). The samples were preconditioned by vacuum saturation before measurement. An example of typical results is given in Figure 9, where concretes having higher packing density (in this case, higher proportions of coarse or fine aggregate, all other factors kept constant) showed a lower chloride transport rate. In general, the concrete samples formulated, based on the packing code, have the highest possible packing density and lowest porosity of their ingredients showed the minimum chloride permeability (*26,27*).

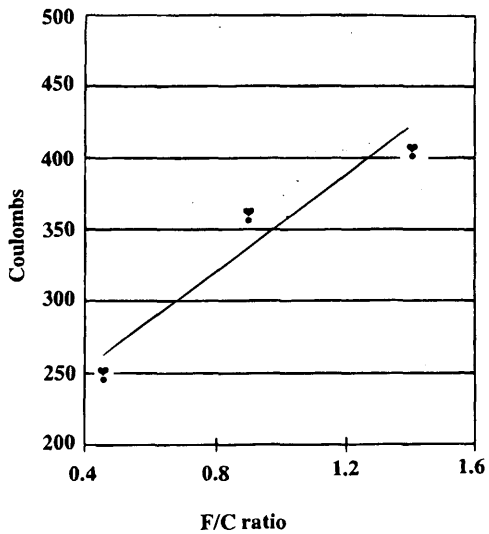

FIGURE 9 Chloride permeability of concrete specimens as measured by monitoring net charge (coulombs) passing in 6 hr through cylinder (95.25ϕ × 51 mm) mounted in cell with two compartments (filled with NaCl and NaOH solutions) under influence of 60 V dc electrical potential (AASHTO T–277).

SUMMARY

Major advances have been made in the development of cementitious materials having superior properties. Such materials have been produced with widely ranging compositions, and their potential applications in modern technology are challenging. High-performance cementitious materials include the very strong, high-density materials of the pressed macro-defect-free (MDF), (DSP), or alkali-activated varieties; their superior properties may be achieved by using either special processing conditions optimal combinations of materials components, or both (*9,21,22*). However, high-performance also includes the ability to predict and achieve long-term durability. The nature of the microstructure of these materials is an important key to such predictability.

This paper has focused on the accomplishments in high-performance cementitious materials with respect to durability. The achievement of dense particle packing, development of a dense microstructure, fine pore structure, superior transport properties, and the relationship among them are critical to high performance and to its understanding and prediction. Additional focus in this important area is critical and will provide new knowledge that will open further horizons in the development of high-performance concrete materials for many applications, especially for the national infrastructure.

ACKNOWLEDGMENTS

The authors acknowledge the support of National Science Foundation (NSF) grant DMR88–12824, the National Academy of Sciences/National Research Council Strategic Highway Research Program grant SHRP–C–201, and NSF grant MSS–91–23239.

REFERENCES

1. *High-performance Construction Materials and Systems: An Essential Program for America and Its Infrastructure*, Civil Engineering Research Foundation, 1993, pp. 20–21.

2. Roy, D. M., Relationships Between Permeability, Porosity, Diffusion and Microstructure of Cement Pastes, Mortar, and Concrete at Different Temperatures *Proc., Materials Research Society Symposium* (L. R. Roberts and J. P. Skalny, eds.). Vol. 137, 1989, pp. 179–189.
3. Neville, A. M. *Properties of Concrete*, 3rd ed. Pitman Publishing Inc., Marshfield, Mass., 1981.
4. Powers, T. C., L. E. Copeland, J. C. Hayes, and Mann, H. M. Permeability of Portland Cement Paste. *Proc., Journal of American Concrete Institute*, Vol. 51; No. 3, 1954, pp. 285–298.
5. Powers, T. C., L. E. Copeland, and H. M. Mann. *Journal for the Portland Cement Association Research and Development Laboratories*, Vol. 1, No. 2, 38, 1959.
6. Nyame, B., and J. Illston. Capillary Pore Structure and Permeability of Hardened Cement Paste. *Proc., 7th International Congress of the Chemistry of Cement*, Vol. 3, 1980, pp. VI–181–185.
7. Shi, D., P. Brown, and S. Kurtz, A Model for the Distribution of Pore Sizes in Cement Paste. *Proc., Materials Research Symposium*, (L. R. Roberts and J. P. Skalny, eds.) Vol. 137, 1989, pp. 23–24.
8. Shi, D., W. Ma, and P. W. Brown, Lognormal Simulation of Pore Evolution During Cement and Mortar Hardening. *Scientific Basis for Nuclear Waste Management*, Vol. 13, Materials Research Society, 1990, pp. 143–148.
9. Roy, D. M., B. E. Scheetz, R. I. A. Malek, and D. Shi. *Concrete Component Packing Handbook*. Supplemental Report 1, SHRP–C–624, Washington, D.C., 1993.
10. Brown, P. W., D. Shi, and J. P. Skalny. Porosity Permeability Relationships. Appendix, Roy, D. M., et al. *Concrete Microstructure Porosity and Permeability*, Supplemental Report 5, SHRP–C–628 SHRP, National Academy of Sciences, Washington, D.C., 1993.
11. Bache, H. H. *Densified Cement/Ultra-Fine Particle-Based Materials*. Cement Beton Laboratory Internal Report 40, CBL, 1981.
12. Scheetz, B. E., J. M. Rizer, and M. Hahn, U.S. Patent No. 4,505,753. 1985.
13. Kumar, A. *Diffusion and Pore Structure Studies in Cementitious Materials*. Ph.D. thesis. Pennsylvania State University, University Park, Pa., 1985.
14. Malek, R. I. A., D. M. Roy, and Y. Fang. Pore Structure, Permeability, and Chloride Diffusion in Fly Ash- and Slag-Containing Pastes and Mortars. *Proc., Materials Research Symposium*, Vol. 137 (L. R. Roberts and J. P. Skalny, eds.), 1989, pp. 403–410.
15. Kumar, A., and D. M. Roy. *Cement and Concrete Research 16*, 1986, pp. 74–78.
16. Li, S., and D. M. Roy. Investigation of Relations Between Porosity, Pore Structure, and Cl Diffusion of Fly Ash and Blended Cement Pastes. *Cement and Concrete Research 16*, 1986, pp. 749–759.
17. Smolcyzk, H. G. State of Knowledge on Chloride Diffusion in Concrete. *Betonwerk und Fertigteil-Technik*, Vol. 12, Germany, 1984.
18. Ushiyama, H., and S. Goto. Diffusion of Various Ions in Hardened Portland Cement Paste. *Proc. 6th International Congress on Chemistry of Cement*, Vol. 2, No. 1, Moscow, Russia, 1974, pp. 331–337.
19. Goto, S., and D. M. Roy. Diffusion of Ions through Hardened Cement Pastes. *Cement and Concrete Research 11*, No. 5, 1981, pp. 751–757.
20. Wise, S., J. A. Satkowski, B. E. Scheetz, J. M. Rizer, M. L. Mackenzie, and D. D. Double. The Development of High Strength Cementitious Tooling/Molding Materials. *Very High Strength, Cement-Based Materials*, Vol. 42 (J. Francis Young, ed.) Materials Research Society, Pittsburgh, Pa., 1985, pp. 245–252.
21. Roy, D. M., P. W. Brown, D. Shi, B. E. Scheetz, and W. Ma. Concrete Microstructure Porosity and Permeability. Supplemental Report 5, SHRP–C–628, SHRP, National Academy of Sciences, Washington, D.C., 1993.
22. Roy, D. M., B. E. Scheetz, and M. R. Silsbee. Processing of Optimized Cements and Concretes via Particle Packing. *MRS Bulletin*, Materials Research Society, Pittsburgh, Pa., 1993, pp. 45–49.
23. Toufar, W., M. Born, and E. Klose. Freeberger Forschungsheft, A559 (VEB Deutschen Verlag fur Grundslaffindustrie), Germany, 1967.
24. Aim, R. B., and P. LeGoff. *Powder Technol*, Vol. 1 1967/1968, pp. 281–290.
25. Roy, D. M., P. D. Cady, S. A. Sabol, and P. H. Licastro. *Concrete Microstructure: Recommended Revisions to Test Methods*. SHRP–C–339. SHRP, National Academy of Sciences, Washington, D.C., 1993.
26. Roy, D. M., and G. M. Idorn. *Concrete Microstructure*. SHRP–C–340. SHRP, National Academy of Sciences, Washington, D.C., 1993.
27. Malek, R. I. A. Effects of Particle Packing and Mix Design on Chloride Permeability of Concrete. *Proc., 9th International Congress on Chemistry of Cement*, Vol. V, National Council for Cement and Building Materials, New Delhi, India, 1992, pp. 143–149.

Publication of this paper sponsored by Committee on Performance of Concrete.